Hittite Journal of Science and Engineering, 2018, 5 (3) 219-223
ISSN NUMBER: 2148-4171
DOI: 10.17350/HJSE19030000098

Microstructure, Corrosion and Wear Properties of FeCrNiMo Based Coating Produced on AISI 1040 Steel by Using Laser Coating Technique

Serkan Islak **Cihan Ozorak**
Kastamonu University, Department of Metallurgical and Materials Engineering, Kastamonu, TURKEY

Article History:
Received: 2017/11/13
Accepted: 2018/03/29
Online: 2018/04/06

***Correspondence to**: Serkan Islak*
Kastamonu University, Department of Metallurgical and Materials Engineering, Kastamonu, Turkey
Tel: 0(212) 473 71 80
E-Mail:serkan@kastamonu.edu.tr

ABSTRACT

This study aims to investigate microstructure, hardness, corrosion and wear properties of FeCrNiMo-based coating produced on AISI 1040 steel by using laser welding method. Microstructure properties and phase formation were examined by SEM-EDS and XRD. The hardness measurement was made by using a microhardness device along a line from the upper surface of the coating to the substrate. The wear tests of both the substrate and coating layer were made with a scratch test device. SEM examinations showed that the coating layer had a dendritic microstructure and was uniformly bonded to the substrate. The coating layer was harder than the substrate. According to wear tests, the friction coefficient of the coating layer was lower compared to the substrate. Substrate and coating layer were immersed in an aqueous solution of %3,5 NaCl for potentiodynamic measurements. Corrosion results showed that coating of the AISI 1040 steel with FeCrNiMo increased the corrosion resistance.

Keywords:
Laser coating, microstructure, wear, corrosion

INTRODUCTION

The wear and corrosion of machine parts is the leading problem encountered in the industry. Surface coating process is widely used to increase corrosion and wear resistance. Many coating methods are used to improve the properties of the surfaces. Basically, coating methods are classified as welding-based coating methods [1,2], thermal spraying [3] and chemical and physical vapor deposition methods [4,5]. Welding-based surface coating methods generally include plasma-transferred arc, gas tungsten arc, laser beam, submerged, electro-slag and electron beam welding processes [6-8]. Laser coating is a unique process that produces a coating metallurgically bonded to the substrate, which finds an increasing application in surface engineering field. A laser beam having a high energy density is a heat source used to melt the coating material and a limited portion of the substrate. The coating materials are in the form of powder, bar or layer. Compared to other coating techniques, laser coating has many advanced properties. These include a metallurgical bonding between the coating and the substrate, a very fine grained microstructure, a low melt rate and a limited heat-affected zone (HAZ) [9-11]. Due to its high corrosion resistance and high wear resistance, the FeCrNiMo alloy is often used under atmospheric conditions in acidic and tribological environments [12]. In this study, a FeNiCrMo based alloy wire was produced as a coating layer on AISI 1040 steel surface by laser welding. Microstructure, phase formation, corrosion and wear properties of the produced coating were investigated.

EXPERIMENTAL STUDIES

AISI 1040 steel in the dimensions of 20 x 10 x 80 mm was used as the substrate material in the surface coating processes. Prior to the laser coating method, the surface of the steel material was cleaned with acetone. Alloy wires with a 0.6 mm diameter were coated on AISI 1040 steel surface by using an Or-Laser brand laser welding machine with the power of 200 Watts. Table 1 shows the chemical composition of the wire and the substrate used in the coating. Fig. 1 shows the the surface coating process with laser welding. The laser coating process was performed in the form of coating passes.

The samples were taken in the dimensions of 10 mm x 10 mm x 10 mm from the middle zone of the coating material for the microstructure examinations and wear test. Coating materials passed through the

Table 1. Chemical composition of substrate and coating wire (wt.%)

Materials	*Cr*	*Ni*	*Mo*	*Mn*	*Co*	*Si*	*C*	*Fe*
Substrate	-	-	-	*0.85*	-	*0.20*	*0.42*	*Balance*
Coating wire	*18*	*10*	*3*	*2.5*	*1.5*	*1*	*0.1*	*Balance*

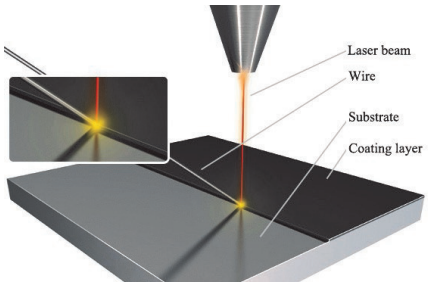

Figure 1. Principle diagram of laser coating process

metallographic processes were etched in 5 ml HNO_3 + 200 ml HCl + 65 g $FeCl_3$ solution for 10 seconds by dipping [13]. SEM-EDS was used for microstructure examinations and XRD was used for phase analysis. The hardness measurement was performed with Future-Tech FM 700 brand micro-hardness device with 200 gr load at 10 sec. waiting period at intervals of 50 µm along a line from the upper surface of the coating to the substrate. Prior to the wear test, the samples were sanded to 1200 mesh sandpaper and their surfaces were polished with a diamond solution and then ultrasonically cleaned. Cleaning was performed with Elma MF3/130KHz device in distilled water for 10 minutes at 35 KHz. Bruker UMT-2-SYS model mechanical test device was used in the wear tests (Fig. 2). The wear was made in the form of micro scratches. A Rockwell indenter was used as the abrasive tip. The scratch size was chosen as 2 mm for all samples. Max 10 N was selected as the load.

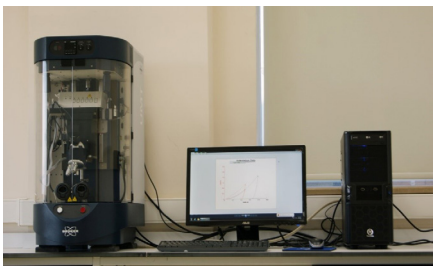

Figure 2. Micro scratch wear device

Corrosion measurements were obtained by using a system consisting of a Reference 3000 Potentiostat / Galvanostat / ZRA corrosion system (Fig. 3). Corrosion experiments were carried out after the samples were left waiting for 1 h at room temperature in a 3.5 wt.% NaCl solution (pH 3). A conventional three-electrode cell was used for all the electrochemical measurements. A saturated calomel electrode (SCE) was used as a reference electrode, platinum foil as a counter electrode and coatings as the working electrode. Potentiodynamic sweeping was performed in range of ± 0.25 V and 1 mV/s sweeping rate. The polarization resistance values were calculated by using Stern and Geary equation.

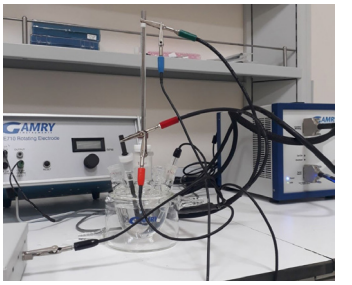

Figure 3. Corrosion system

RESULTS AND DISCUSSION

Fig. 4 shows SEM images of the FeCrNiMo-based coating produced on the AISI 1040 steel surface by the laser welding. The coating thickness was observed to be about 250 µm (Fig. 4a). It is also clearly seen in the same SEM image that the coating layer was composed of overlapped multi-passes. Coating layer formed of cellular structure and dendritic structure. Dendrites occurred in the opposite direction of the heat flow (Fig. 4b). This coating microstructure contained austenite and α-ferrite. Approximate ratio of these structures was determined by means of the Schaeffler diagram in Fig. 4c. These structures formed as solid solutions. No pore or crack formation was found in the coating layer. MAP-EDS analysis was carried out to see how the element distribution in the coating layer is, which is shown in Fig. 5. There was a homogeneous distribution in the coating layer. No oxide formation occurred.

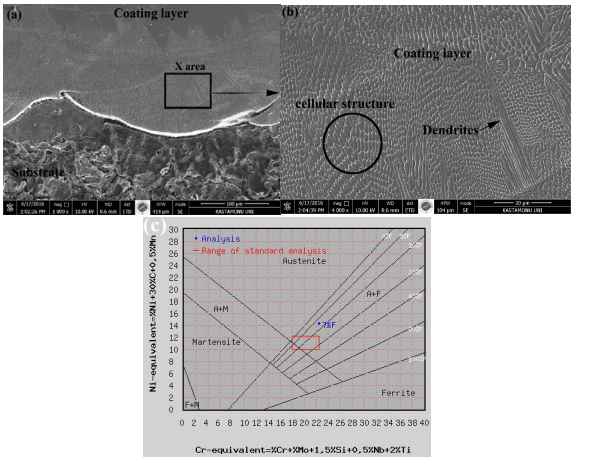

Figure 4. (a) Coating and substrate, (b) coating area (X area) and (c) Schaeffler diagram

Fig. 6 shows the regional EDS analysis of the coating layer. The basic element of the coating layer was iron. The other elements were Cr, Ni, Mo, Mn, and Co. The chemical composition of the coating layer was similar to the chemiv-

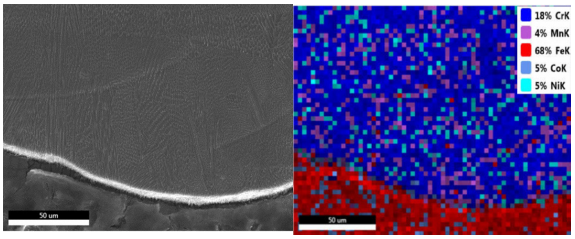

Figure 5. MAP-EDS analysis

cal composition of the selected coating wire. This indicated that the coating process reached its goal. In order to show the elemental difference between the coating layer and substrate, line EDS was performed between the coating and substrate. Fig. 7 shows line EDS. Cr, Ni, and Mn elements increased significantly in the coating layer.

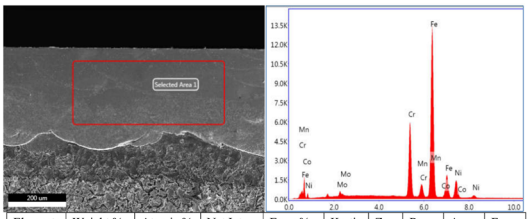

Elements	Weight %	Atomic %	Net Int.	Error %	Kratio	Z	R	A	F
CrK	17.63	19.02	4,112.44	2.65	0.21	1	0.99	0.97	1.22
MnK	2.20	2.25	407.93	5.15	0.02	0.98	0.99	0.98	1.09
FeK	65.88	66.18	10,211.89	1.99	0.63	1	1	0.92	1.04
CoK	1.31	1.25	178.29	11.25	0.01	0.98	1	0.92	1.04
NiK	10.03	9.59	1,128.97	4.27	0.08	1.02	1.01	0.8	1.04
MoK	2.95	1.72	16.42	58.63	0.04	0.87	1.04	0.99	1.45

Figure 6. EDS analysis of the coating layer

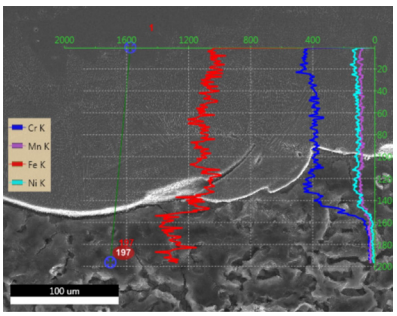

Figure 7. ELine EDS analysis between coating and substrate

Fig. 8 shows the XRD analysis of the coating produced on the AISI 1040 steel surface by the laser welding. The coating layer consisted of α-Fe (ferrite), γ-Fe (austenite) and M23C6 phases. The letter M represents the elements Fe, Cr, and Mo. While austenite peak occurred at the angle of 43.6, 50.6 and 74.7 2θ angles, the ferrite peak occurred at the angles of 64.9 and 81.9 2θ. The intensity of the M23C6 carbide peak was very low compared to the other two phases. The phases occurring in this study are also similar to those in the literature [14]. Since the coating layer had Cr-Ni content, no oxide phase was found. This shows that it is corrosion resistant.

Fig.9 shows the hardness of the coating layer. The microhardness measurement of the coating layer was carried

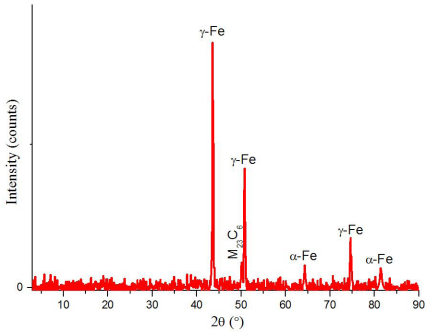

Figure 8. XRD graph of laser coated layer

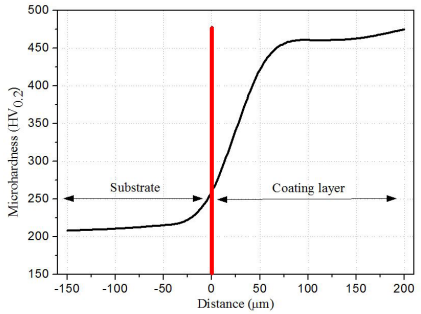

Figure 9. Hardness transition from the coating layer to substrate and the red line transition border

out depending on the distance. There was a significant increase in hardness value of the coating layer compared to the substrate. While the hardness of the substrate was about 210 HV0.2, the hardness of the coating layer was measured as 475 HV0.2. The increase measured was 2 times compared to the substrate. The increase in the hardness of the coating layer was associated with the effect of the mechanism increasing the solid solution strength and the dispersion strengthening of the carbides.

Wear test of the coating layer and the substrate was conducted in the form of micro-scratches. A Rockwell indenter was used as the abrasive indenter. The scratch size was chosen as 2 mm in both samples. Fig. 10 shows wear graphs showing the friction coefficients of the coating layer and substrate. The applied load was measured as 9.55 N, which was maximum. The wear test was completed in 14 seconds. Friction coefficient graphs were also drawn as friction coefficient versus time. When the graph was examined, it was understood that the friction coefficient of the coating layer (~0.17) was lower than the friction coefficient of the substrate (~0.23). This decrease was associated with the solid solution strengthening and the dispersion strengthening of the carbides. Fluctuations were observed in the friction coefficient values of the coating layer. This was related to the fact that the phases were not homogeneously distributed in some regions of the coating. Fig. 11 shows optical images of the wear marks. It was seen that plastic deformation was more intense in the substrate. Flaking was observed in both wear marks. Gong et al [15] presented a study on influence

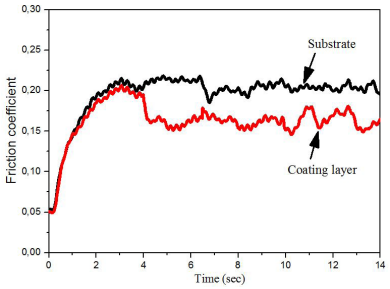

Figure 10. Time-dependent coefficient of friction graph of the samples

of heat treatment on microstructure and mechanical properties of FeCrNi coating produced by laser cladding. The results of the study showed that as the heat treatment temperature increased, the wear resistance decreased although

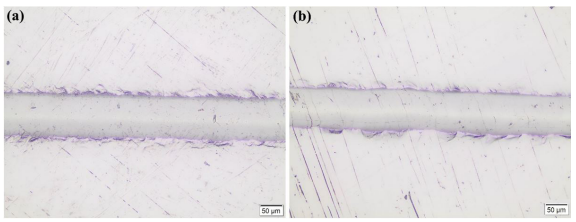

Figure 11. Wear tracks; (a) the substrate and (b) the coating

the maximum tensile strength was obtained.

The potentiodynamic polarization curves of the substrate and coating layer are illustrated in Fig. 12. The corrosion measurement data are summarized in Table 2. Corrosion potential (E_{corr}), anodic and cathodic Tafel slopes (β_a and β_c), corrosion resistance (R_p), corrosion rate and corrosion current (I_{corr}) were found from Tafel curves. Rp was calculated by the Stern and Geary equation [16].

$$Icorr = \frac{\beta_a . \beta_c}{2.303 x R_p \left(\beta_a + \beta_c\right)}$$

where I_{corr} is the corrosion current density in μA cm^{-2}, R_p is the corrosion resistance in kΩ cm^2, and β_a and β_c are the anodic and cathodic Tafel slopes in V or mV, respectively. The corrosion potential (E_{corr}) values of the substrate and coating layer are slightly different. While Ecor of substrate is -435 mV, Ecorr of coating layer is -293 mV. The (R_p of the substrate and coating layer are 20,70 kΩ.cm^2 and 25,57 kΩ.cm^2, respectively. R_p of the coating layer was increased by about 23,4 % compared to that of the substrate. The key element that determines the corrosion resistance of the coating layer is chromium. Cr forms a very thin film on the surface of the material against corrosion attacks. The protective film called passive layer or passive film [17]. The Ni element has a regulatory effect on the ductility and toughness properties of the material. The Mo element provides the continuity of the passive layer formed to protect from corrosion [18, 19]. Qiao et al [20] studied the corrosion behavior of HVOF-sprayed Fe-based alloy coating in various solutions. It has been observed that the coating layer exhibits different corrosion resistances in different solutions. However, it has been reported that the coating layer has higher corrosion resistance than the bottom layer. Our study showed similar results with these results.

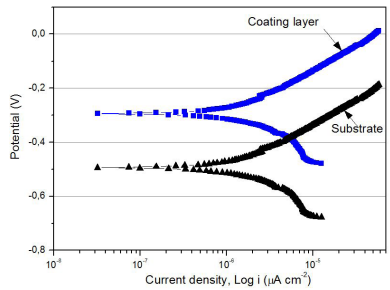

Figure 12. The potentiodynamic polarization curves of substrate and coating layer

Table 2. Electrochemical results of substrate and coating layer

Materials	*E_{cor} (mV)*	*Icor (μAcm⁻²)*	*βa (mV)*	*βc (mV)*	*Corrosion rate (mpy)*	*Rp (kΩ.cm²)*
Substrate	*-435*	*2.35*	*201.8*	*235.2*	*990.2*	*20.70*
Coating wire	*-293*	*2.01*	*235.1*	*238.3*	*945.1*	*25.57*

CONCLUSION

1. In this study, FeCrNiMo based alloy wire was successfully coated on AISI 1040 steel surface with the laser welding technique.
2. It is seen from the SEM images that the coating had dendritic and cell morphology. This shows similarity with the literature. According to the XRD analyses, α-Fe (ferrite), γ-Fe (austenite) and M23C6 phases formed as phases in the structure. It was also found by the Schaeffler diagram that these phases can form. Majority of the structure had an austenite character.
3. The hardness of the coating layer was about two times more than that of the substrate. This increase in the hardness was caused by solid solution and M23C6 carbides formed in the structure.
4. Wear tests of the coating layer and the substrate were made in the form of micro-scratches. A decrease was experienced in the friction coefficient of the coating layer compared to the substrate. This was caused by strength increasing mechanisms.
5. The corrosion potentials of the substrate and coating layer are slightly different. Coating of FeCrNiMo on AISI 1040 steel has increased corrosion resistance by 23,4 %. Cr contributes directly to the corrosion resistance, whereas Mo contributes indirectly.

REFERENCES

1. Deuis RL, Yellup JM, Subramanian C. Metal–matrix composite coatings by PTA surfacing. Composites Science and Technology 58 (1998) 299–309.

2. Gülenç B, Kahraman N. Wear behaviour of bulldozer rollers welded using a submerged arc welding process. Materials & Design 24 (2003) 537–542.
3. Nakajima A, Mawatari T, Yoshida M, Tani K, Nakahira A. Effects of coating thickness and slip ratio on durability of thermally sprayed WC cermet coating in rolling/sliding contact. Wear 241 (2000) 166–173.
4. Knight JC, Page TF. The fine–scale microstructure of thin hard TiN and TiC coatings on steels. Thin Solid Films 193–194 (1990) 431–441.
5. Wolfe DE, Singh J, Narasimhan K. Synthesis of titanium carbide/chromium carbide multilayers by the co–evaporation of multiple ingots by electron beam physical vapor deposition. Surface and Coatings Technology 160 (2002) 206–218.
6. Budinski KG. Hardsurfacing: an overview of the process. Welding Design & Fabrication, July (1986) 51–57.
7. Buytoz S., Orhan A., Gur A.K., Caligulu U. Microstructural Development of Fe-Cr-C and B4C Powder Alloy Coating on Stainless Steel by Plasma–Transferred Arc Weld Surfacing. Arabian Journal for Science and Engineering. 38(8) (2013) 2197–2204.
8. Wu W, Hwu LY, Lin DY, Lee JL. The Relationship between alloying elements and retained austenite in martensitic stainless–steel welds. Scripta Materialia 42 (2000) 1071–1076.
9. Pei YT, Zuo TC. Gradient microstructure in laser clad TiC–reinforced Ni–alloy composite coating. Materials Science and Engineering A 241 (1998) 259–263.
10. Yang S, Liu WJ, Zhong ML, Wang ZJ. TiC reinforced composite coating produced by powder feding laser cladding. Mater. Lett. 58 (2004) 2958–2962.
11. Anandkumar R, Almeida A, Colaço R, Vilar R, Ocelik V, De Hosson JThM. Microstructure and wear studies of laser clad Al–Si/SiC(p) composite coatings. Surface & Coatings Technology 201 (2007) 9497–9505.
12. Ratajski T, Kalemba–Rec I, Dubiel B. Manufacturing, Microstructure and Corrosion Resistance of Electrophoretically Deposited SiO2 and Ni/SiO2 Coatings on X2CrNiMo17-12-2 Steel. Archives of Metallurgy and Materials. 61(2) (2016) 1221-1227.
13. ASTM E407–07. "Standard Practice for Microetching Metals and Alloys." (2015): 1–4.
14. Sun SD, Fabijanic D, Ghaderi A, Leary M, Toton J, Sun S, Brandt M, Easton M. Microstructure and hardness characterization of laser coatings produced with a mixture of AISI 420 stainless steel and Fe–C–Cr–Nb–B–Mo steel alloy powders, Surface and Coatings Technology, 296 (2016) 76–87.
15. Gong, Fu–bao, et al. Influence of heat treatment on microstructure and mechanical properties of FeCrNi coating produced by laser cladding. Transactions of Nonferrous Metals Society of China 26.8 (2016): 2117–2125.
16. Stern M, Geary AL. Electrochemical Polarization I. A Theoretical Analysis of the Shape of Polarization Curves. Journal of The Electrochemical Society 104 (1957) 56.
17. George G, Shaikh H. Introduction to Austenitic Stainless Steels, Corrosion of Austenitic Stainless Steels. Mechanism, Mitigation and Monitoring, edited by: H. S. Khatak, B. Raj, Woodhead Publishing House, Cambridge, UK, (2002).
18. Sedriks AJ, Corrosion of Stainless Steels, Wiley, New York, NY, USA, 2nd edition, (1996).
19. Porcayo–Calderon J, Casales–Diaz M, Salinas–Bravo VM, Martinez–Gomez L. Corrosion Performance of Fe–Cr–Ni Alloys in Artificial Saliva and Mouthwash Solution. Bioinorganic Chemistry and Applications 2015 (2015) 1–14.
20. Qiao L., Wu Y., Hong S., Qin Y., Shi W., Li G. Corrosion Behavior of HVOF–Sprayed Fe–Based Alloy Coating in Various Solutions. Journal of Materials Engineering and Performance, 26(8) (2017) 3813–3820.